Article

3D Framework Carbon for High-Performance Zinc-Ion Capacitors

Setthathon Kiatikajornjumroen , Xiaopeng Liu , Yinan Lu , Buddha Deka Boruah *

Posted Date: 26 June 2023

doi: 10.20944/preprints202306.1789.v1

Keywords: Pyrolysis; porous carbon; zinc ion capacitor

Article

3D Framework Carbon for High-Performance Zinc-Ion Capacitors

Setthathon Kiatikajornjumroen[1], Xiaopeng Liu[1], Yinan Lu[1] and Buddha Deka Boruah[1,*]

[1] Institute for Materials Discovery (IMD), University College London (UCL), London, WC1E 7JE, UK
* Correspondence: Dr. Buddha Deka Boruah: b.boruah@ucl.ac.uk

Abstract: With the rapid and continuous advancement and deployment of advanced energy storage devices, there has been significant interest in aqueous capacitors that possess non-flammable properties and high safety features. Consequently, extensive research efforts have focused on investigating zinc anodes and low-cost carbonaceous cathode materials. Despite these efforts, the development of high-performance zinc-ion capacitors (ZICs) still faces challenges such as limited cycling stability and low energy densities. In this study, we present a novel approach to address these challenges. We demonstrate the utilization of a three-dimensionally (3D) grown conductive porous carbon framework cathode coupled with zinc anode cells, which exhibit exceptional stability and durability in ZICs. Our experiments reveal a remarkable cycling performance, with a capacity retention of approximately 97.3% and a coulombic efficiency of nearly 100% even after 10,000 charge-discharge cycles. These findings signify significant progress in enhancing the performance of ZICs.

Keywords: Pyrolysis; porous carbon; zinc ion capacitor

1. Introduction

Rechargeable energy storage devices with low cost and long cycle life are essential for the development of the sustainable economy [1]. With intermittent renewable energy such as sunlight and wind from nature, batteries and supercapacitors (SCs) store them for future utilization [2]. Among various choices, aqueous zinc-ion capacitors (ZICs) have attracted great interest owing to their inherent advantages of balancing the gap between high energy density of batteries and high power density of SCs [3 – 5]. As a typical anode material in ZICs, zinc metal shows a high theoretical gravimetric/volumetric capacity (823 mAh g^{-1}; 5851 mAh cm^{-3}), and also a low redox potential (−0.76 V) [6]. In addition, aqueous electrolytes used in ZICs offers the system high safety and low cost [7]. Given these merits, ZICs show great potential to be developed for broad real-world applications. However, the commercialization of the device is hindered by the high production cost and interior cycling stability of porous carbon cathode, which play decisive roles in the energy and power characteristics of the ZICs [8, 9].

To pursue high-performance ZICs, remarkable advances have been made in the development of porous carbon material and there were many successful carbon electrodes have been engineered via various synthesis routes. For instance, Shang et al. synthesized a nitrogen-enriched mesoporous carbon nanosheets (NPCNs) cathode by a urea-mediated foaming strategy to enhance the conductivity, which increases charge transfer efficiency and reduces side reactions during zincation [10]. Deng and co-workers reported a N, O co-doped hierarchical porous carbon (HPC) cathode for ZIC. The fabricated device showed high specific capacity of 138.5 mA h g^{-1} and an excellent cycle lifetime that without capacity decay after 10 000 cycles [11]. Some researchers engineered the carbon structure into various morphologies and used of low entropy carbonaceous structures like graphene and graphite, which offers good crystallinity leading to enhanced life cycling stability [12 – 15]. However, there were various complex process that requires high temperature and aggressively toxic chemical processing in carbon derivation and treatment, which are essential multi-step carbonization that increases the cost of electrode powder preparation [16, 17]. To achieve practical application of

Preprints (www.preprints.org) | NOT PEER-REVIEWED | Posted: 26 June 2023 doi:10.20944/preprints202306.1789.v1

ZICs, it is urgent to explore a simple and cheap process to synthesize porous carbon cathode for high-performance ZICs.

In this work, three-dimensionally (3D) growth of a conductive porous carbon framework cathode was obtained via direct pyrolysis of sodium citrate. The porosity structure of the electrode benefits to ion diffusion and thus excellent rate capability. Moreover, the porous carbon framework showed superior cycling stability that maintained a capacity of 97.3% after 10 000 cycles at 10 A g^{-1} and excellent reversible rate capability with a higher recovery rate.

2. Materials and Methods

Porous Carbon Derivation: For the preparation of porous carbon, sodium citrate is placed onto the alumina sample container and slid into the quartz tube inside a Eurotherm-3216-3208-3204 PID Built-in Elite Thermal Systems Limited controlled atmospheric furnace equipment. The furnace is programmed to heat and hold the sample up to 500 ^{o}C for 30 minutes at step 1 and then in step 2, heat it to 650 ^{o}C and hold for 1 hour and cool it down. Before the heating, the argon gas is purged into the quartz tube at 2 PSI for 30 minutes to produce an argon atmosphere and reduce oxygen content.

After the sodium citrate has been completely pyrolyzed and cooled down to room temperature, the samples are removed, which are left with only tar, charcoal, and sodium-based salts (Na_2CO_3). The samples are placed into the beaker with deionized water sufficiently to fill the beaker volume and heated by a heater plate inside a fume hood at 80 ^{o}C for 30 minutes to remove the salt inside the porous carbon. Then the vacuum filtration equipment is set up using Whatman filter paper to capture the porous carbon. The warm solution in the beaker is poured into the vacuum filtration slowly. Once the product is completely filtered, add ethanol solvent until the equipment filters all the ethanol followed by adding more warm water to remove residual salts for 3 times. After that, the samples on the Whatman filter paper are placed into the glass petri dish and placed inside the vacuum furnace, and set program at 100 ^{o}C to leave overnight. Then the obtained porous carbon is placed into the Thinky Mixer Model ARM-310 vessel with 6 zirconia balls (6.4987 g) to operate the mixer at 2000 RPM for 30 minutes.

Material Characterization: The morphology of powder samples was analyzed by Oxford Instrument Wave ZEISS Scanning Electron Microscopy. The lattice and phase structure of powder samples were determined by X-ray diffraction (AERIS PANalytical for XRD diffraction characterization with XRD source of Cu Ka.) from 10° to 80°. The bonds of the porous carbon were inspected by FTIR (Perkin-Elmer). Further, Raman (Renishaw) and BET surface area (Quantachrome) characterizations were explored to analyze the samples.

Cell Assembly: The cathode slurry was then obtained by mixing all the active materials, Super P Conductive and PVDF binder in a ratio of 70wt%:20wt%:10wt% using a Thinky Mixer Model ARM-310. After that, a homogenized slurry was drop cast on carbon felt current collectors and dried overnight at 70 °C under a vacuum oven. Then, the cells were assembled in a CR2032 coin cell with 0.25 mm zinc anode foil metal against a porous carbon electrode with a glass fibre Whatman porous separator with 3M $Zn(CF_3SO_3)_2$ aqueous electrolyte in an open atmosphere. The cells were then rested for 10 hours prior to electrochemical characterization.

Electrochemical Performance: The electrochemical performances of the ZIC were tested by using Biologic VMP-3, Neware Battery Testing System and Gramry Instruments Interface 1010E potentiostats. The Cyclic voltammetry (CV) measurement at different scan rates (10 – 1000 mV s-1) and galvanostatic charge–discharge performances at different specific currents (0.1 – 20 A g^{-1}) were over a voltage range of 0.2 – 1.8 V. Long-term cycling test measured at 10 A g^{-1} for 10,000 cycles using a Neware Battery Testing System. Electrochemical impedance spectrum (EIS) measurements were also measured using EIS Gramry Instruments Interface 1010E Potentiostat/Galvanostat/ZRA 21128 with program Gramry Framework in the frequency range 10 mHz – 100 kHz at 10 mV voltage amplitude.

 doi:10.20944/preprints202306.1789.v1

3. Results

The schematic synthesis procedure for the direct pyrolysis of sodium citrate was presented in Figure 1a-c. Porous carbon could be obtained by a self-assembly procedure. In brief, sodium citrate was heated directly in the tube furnace, where it decomposed gradually and left only carbon in the structure. The carbon self-assembled with each other and formed porous carbon eventually. Figure 1d showed the Raman spectrum of porous carbon. The D-band (disorder) and G-band (graphitic carbon) showed around 1345 and 1580 cm^{-1} are the characteristic peaks of amorphous carbon [18]. The intensity ratio (I_D/I_G) was measured to be 1.3, which confirmed the acceptable graphitization degree of our as-prepared porous carbon. The D band could be attributed to the sp3-hybridized carbon while the G band was related to ordered graphitic sp2-hybridized carbon [19]. The surface area and porous structures of the as-prepared porous carbon were then evaluated by N_2 adsorption/desorption measurements. Figure 1e illustrated a typical type N_2 adsorption/desorption isotherm with a measured specific surface area is 194.65 $m^2\ g^{-1}$.

The scanning electron microscopy (SEM) image of the as-pyrolyzed sodium citrate samples displayed 3D porosity structure of porous carbon (Figure 2a,b). The rod like morphology tends to be sodium carbonate that is left with carbon nanosheets. Compared with as-pyrolyzed sodium citrate, the generation of 3D porous carbon was observed after dissolving as-pyrolyzed sodium citrate (Figure 2c,d). Figure 2e provided the XRD patterns of the as-prepared sodium citrate and porous carbon. The characteristic peaks observed from XRD patterns corresponded to the lattice planes of (002), (310), (112) and (400) of sodium carbonate material, which are matched with the JCPDS card no. 72-0628 [20]. The characteristic diffraction peaks at $2\theta = 26°$ and 43° were responsible for the lattice planes of (002) and (101) of carbon material (JCPDS no. 41-1487), and also indicated that amorphous carbon was embedded inside sodium carbonate [21]. Figure 2f showed the FTIR spectra for pyrolyzed sodium citrate and porous carbon in the range of 4000-500 cm^{-1}. For pyrolyzed sodium citrate, the absorption peaks at 695, 879, 1412, 1774, and 3310 cm^{-1} corresponded to the vibrational bond for C-O-C, C-C, C=O, O=C=O and C-OH, respectively [22]. These findings demonstrated that hydrocarbons were generated during and after pyrolysis of sodium citrate and the existence of carbonate-based material could be confirmed by carbon-oxygen peaks in the spectra. The peaks for C-C bond were associated with the carbon embedment inside the sodium carbonate. After the salt are dissolved to form porous carbon, the peaks for C-C (carbon) and C-OH (hydroxy) appeared in the porous carbon spectrum, which indicated that there was residue contamination from salt and ethyl alcohol left after being used for dissolving salts. The C-OH group still occurred due to water–carbon interaction which leads to the surface of the carbon bond modification which forms hydroxy bonds, while C=O=C forms due to interaction with oxygen.

Preprints (www.preprints.org) | NOT PEER-REVIEWED | Posted: 26 June 2023 doi:10.20944/preprints202306.1789.v1

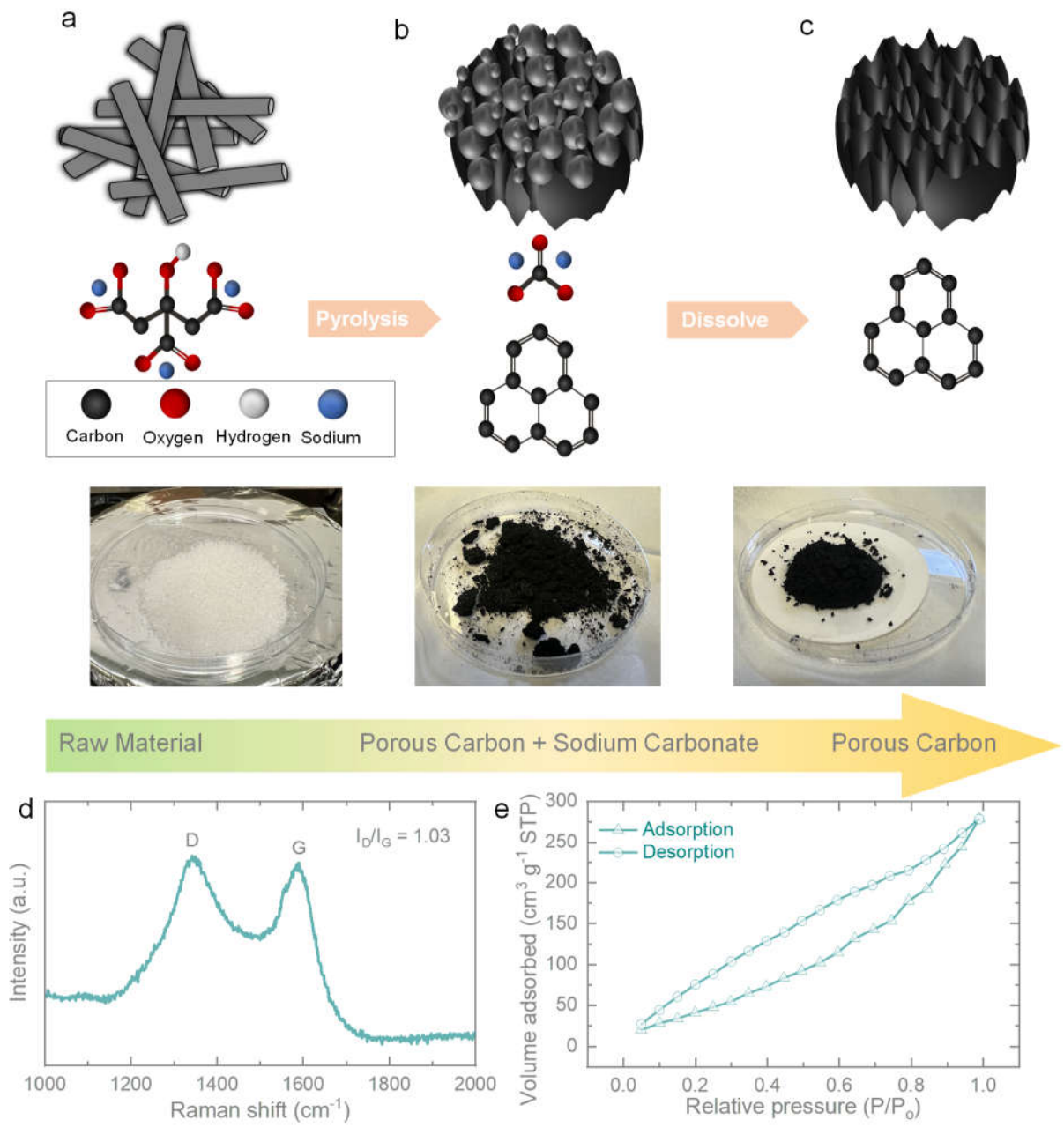

Figure 1. Schematic representing (a-c) diagram of porous molecular and structural transformation that causes the pyrolyzed sodium citrate to form porous carbon as a cathode. The below images are digital photographs of the raw material, pyrolyzed sodium citrate, and porous carbon image. (d, e) Raman and N_2 adsorption-desorption isotherms of porous carbon.

Preprints (www.preprints.org) | NOT PEER-REVIEWED | Posted: 26 June 2023 doi:10.20944/preprints202306.1789.v1

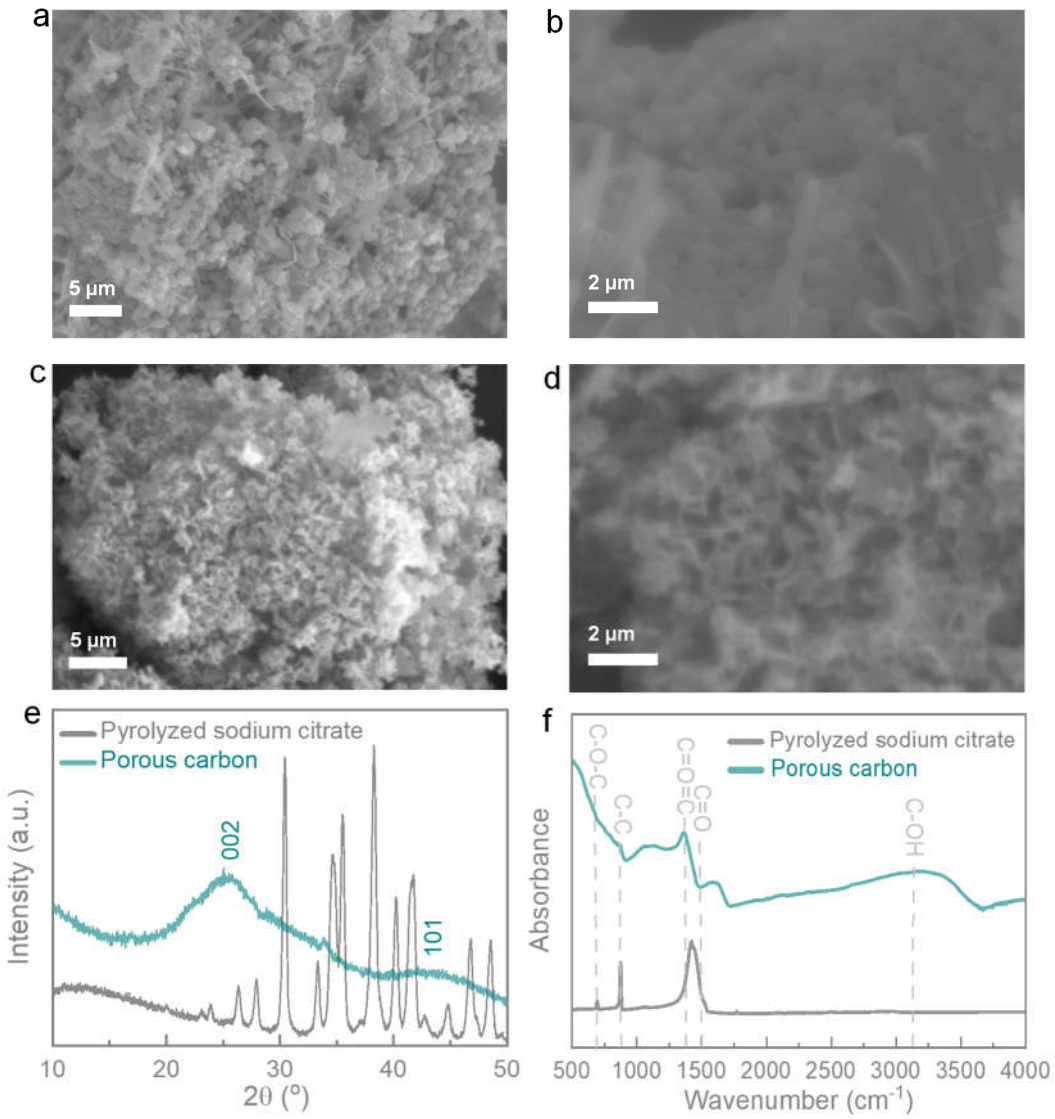

Figure 2. (a, b) SEM image of pyrolyzed sodium citrate at low and high magnifications. and porous carbon at a magnification of 20K, respectively. (c, d) SEM images of porous carbon at low and high magnifications, respectively. (e, f) XRD patterns and FTIR curves, respectively for pyrolyzed sodium citrate and porous carbon.

To illustrate the charge storage performance of ZIC, Figure 3a showed Cyclic Voltammetry (CV) measurements over a voltage window between 0.2 and 1.8 V at various scan rates of 10 – 100 mV s^{-1}. The CV curves exhibited similar shape redox at different scan rates, which showed excellent rate capability even at a high scan rate of 1000 mV s^{-1} (Figure 3b). The rectangular shapes were kept well and did not display obvious deformation in rectangular patterns at various scan rates. To confirm the stability of the as-prepared porous carbon, the CV curves of ZIC at 1000 mV s^{-1} for 10,000 cycles was shown in Figure 3c. It could be seen that the curves overlapped without obvious change through 10,000 cycles, which indicated high charge transfer efficiency and high stability of our porous carbon. Figure 3d showed the Nyquist plot of porous carbon, where the semi-circular curves in the high-frequency range could be attributed to the charge transfer resistance (Rct), while lower equivalent series resistance (Rs) was related to the slope lines in the low-frequency region. ZIC exhibited Rct of 130.04 Ω and Rs of 2.03 Ω. The electrode showed nearly unimpeded ion diffusion, which benefits from 3D porous structure of the material.

Preprints (www.preprints.org) | NOT PEER-REVIEWED | Posted: 26 June 2023 doi:10.20944/preprints202306.1789.v1

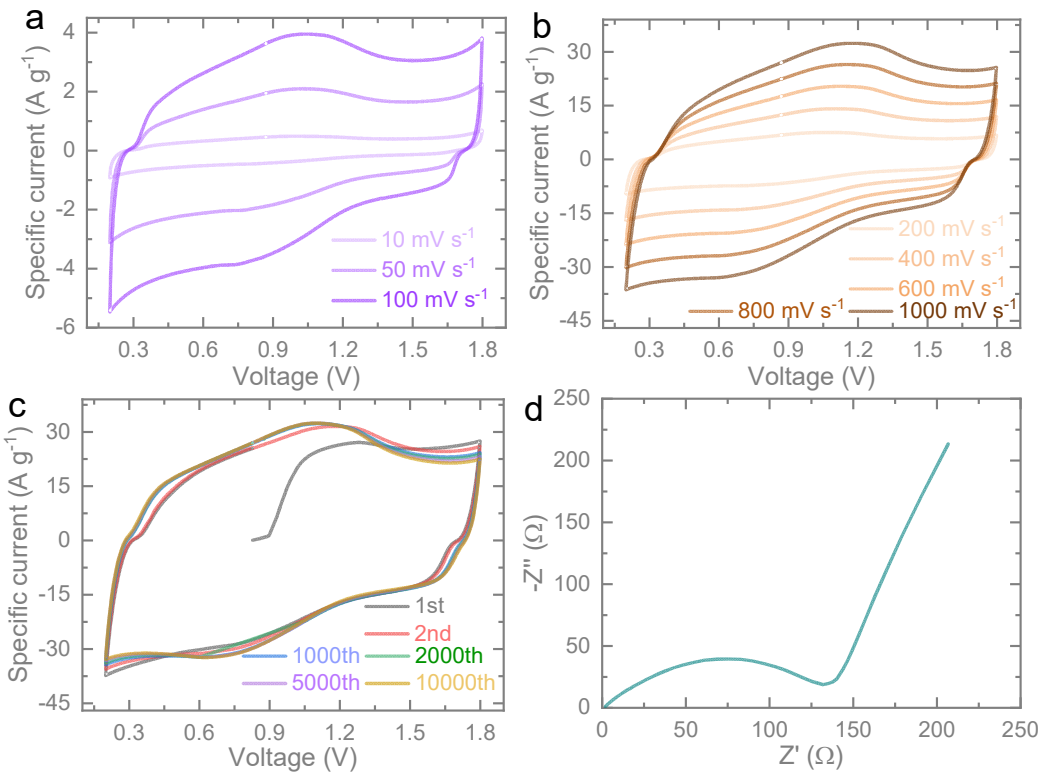

Figure 3. Graphical result for the electrochemical test including CV measurement at (a) 10 – 100 mV s^{-1} and (b) 200 – 1000 mV s^{-1} in a voltage window 0.2 – 1.8 V. (c) Cycling CVs at 1000 mV s^{-1} for 1st, 2nd,1000th, 2000th, 5000th and 10,000th cycles. (d) EIS (electrochemical impedance spectroscopy) measurement of the Zn//PC measured in the frequency range of 10 mHz to 100 kHz at a voltage amplitude of 10 mV before cycling.

Figures 4a and b display the galvanostatic charge-discharge curves of ZIC. From the high symmetry in the anodic charging section and the corresponding cathodic discharging segment in the galvanostatic charge-discharge curve, a highly reversible capacitive material was proved. When the current density adds up to a maximum of 20 A g^{-1}, the capacitance retention is kept well. In the case of large current density (Figure 4b), the interaction between diffusion ions and electrodes in the electrolyte tends to limit and induced the decrease of specific capacitance.

The rate capability measurement was measured to assess the energy storage capability of a ZIC at Figure 4c. The specific capacities of ZIC are 32.05, 21.20, 16.87, 14.72, 13.15, 11.54, 10.51, 9.40 and 14.80 mAh g^{-1} at specific currents of 0.1, 0.2, 0.5, 1.0, 2.0, 5.0, 10.0, 20.0 and 1.0 A g^{-1}, respectively. When the current density returns to 1.0 A g^{-1}, the capacity of 14.80 mAh g^{-1} can be maintained with a recovery rate of up to 99.46%. This demonstrates that porous carbon-based capacitor offers good reversible rate capability. Here in Figure 4d, our ZIC exhibited stable cycling performance for 10,000 cycles at a specific current of 10 A g^{-1}, the capacity retention of 97.3% and coulombic efficiency of nearly 100% were achieved, so it could be depicted that porous carbon cathode can supply highly stable electrochemical reversibility at long life cycling. The percentage retention capacity drop was credited to the formation of a thin passivation layer on the zinc anode, which impeded the interfacial transportation of zinc ions. Throughout the cycles, the retention drop was accredited to more dendrites on the zinc anode. There was a minor degradation of specific capacitance at initial cycles in ZIC electrodes. However, the overall cycling performance trend demonstrated that porous carbon exhibits a superior stable and long cycling life electrode-specific capacity.

Preprints (www.preprints.org) | NOT PEER-REVIEWED | Posted: 26 June 2023 doi:10.20944/preprints202306.1789.v1

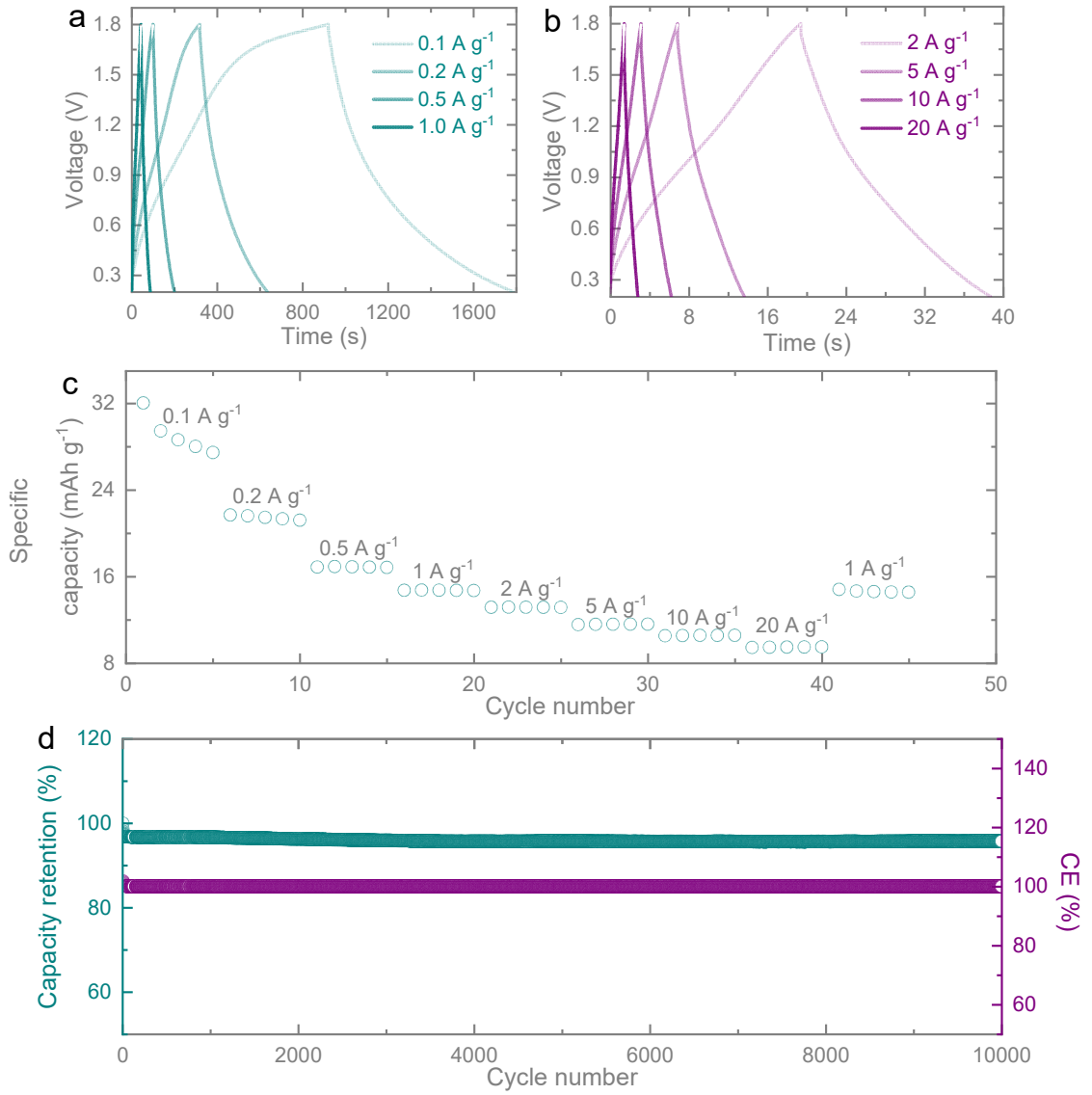

Figure 4. (a) Galvanostatic charge-discharge curves at specific currents of (a) 0.1 – 1.0 A g^{-1} and (b) 2 – 20 A g^{-1} recorded in a voltage window of 0.2 – 1.8 V. (c) Rate capability test of the Zn//PC cell at specific currents of 0.1, 0.2, 0.5, 1.0, 2.0, 5.0, 10.0, 20.0 and 1.0 A g^{-1} for 5 cycles at each specific current. (d) Graphical results for the electrochemical test including the long-term cycling performance at a current density of 10 A g^{-1} for 10,000 cycles, which illustrates the capacity retention and coulombic efficiency (CE) curves.

4. Conclusions

In summary, the 3D growth of a conductive porous carbon framework cathode was synthesized by the thermal decomposition of sodium citrate followed by carbonization. The 3D porosity structure provides the electrode with more ion transportation channels that reduce the transport resistance by reducing the diffusion pathways. As a result, the zinc ion capacitor exhibited an outstanding reversible rate capability with a recovery rate of 99.46% after returning from 20 A g^{-1} to 1 A g^{-1}, and a stable cycling performance that capacity retention of 97.3% after 10 000 cycles at 10 A g^{-1}. This work provides a single-step route to synthesize high-performance porous carbon cathodes for ZICs.

Supplementary Materials: No applicable.

Author Contributions: Conceptualization, S.K. and B.D.B.; methodology, S.K.; validation, S.K., X.L. and Y.L.; investigation, S.K. X.L and Y.L.; resources, B.D.B.; data curation, S.K., X.L. and Y.L.; writing—original draft preparation, S.K., X.L. and B.D.B.; writing—review and editing, , S.K., X.L., Y.L. and B.D.B.; supervision, B.D.B. All authors have read and agreed to the published version of the manuscript.

Funding: This research received no external funding.

Institutional Review Board Statement: Not applicable.

Informed Consent Statement: Not applicable.

Data Availability Statement: The Data used in this study are available on request.

Acknowledgments: Not applicable.

Conflicts of Interest: The authors declare no conflict of interest.

References

1. Kandambeth, S.; Kale, V. S.; Shekhah, O.; Alshareef, H. N.; Eddaoudi, M. 2D Covalent-Organic Framework Electrodes for Supercapacitors and Rechargeable Metal-Ion Batteries. *Adv. Energy Mater.* **2022**, *12*, 2100177.
2. Boruah, B. D.; Mathieson, A.; Park, S. K.; Zhang, X.; Wen, B.; Tan, L.; Boies, A.; Volder, M. D. Vanadium Dioxide Cathodes for High-Rate Photo-Rechargeable Zinc-Ion Batteries. *Adv. Energy Mater.* **2021**, *11*, 2100115.
3. Boruah, B. D.; Wen, B.; Volder, M. D. Molybdenum Disulfide–Zinc Oxide Photocathodes for Photo-Rechargeable Zinc-Ion Batteries. *ACS Nano* **2021**, *15*, 16616-16624.
4. Gong, X.; Chen. J.; Lee, P. S. Zinc-Ion Hybrid Supercapacitors: Progress and Future Perspective. *Batter. Supercaps.* **2021**, *4*, 1529-1546.
5. Boruah, B. D.; Wen, B.; Volder, M. D. Light Rechargeable Lithium-Ion Batteries Using V2O5 Cathodes. *Nano Lett.* **2021**, *21*, 3527-3532.
6. Chen, X.; Zhang, H.; Gao, Y.; Liu, J. H.; Cao, X.; Zhan, C.; Wang, S.; Wang, J.; Dou, S. X.; Cao, D. Zinc-ion hybrid supercapacitors: Design strategies, challenges, and perspectives. *Carbon Neutralization* **2022**, *1*, 159-188.
7. Patil, S. J.; Chodankar, N. R.; Hwang, S.-K.; Shinde, P. A.; Rama Raju, G. S.; Ranjith, K. S.; Karekar, S. V.; Huh, Y.-S.; Han, Y.-K. Two-dimensional nanosheets of bimetallic chalcogenide-tagged nitrogen-doped carbon as a cathode for high-performance and durable zinc-ion capacitors. *J. Mater. Chem A* **2023**, *11*, 5112-5126.
8. Zhang, D.; Li, L.; Gao, Y.; Wu, Y.; Deng, J. Carbon-Based Materials for a New Type of Zinc-Ion Capacitor. *ChemElectroChem* **2021**, *8*, 1541-1557.
9. Yin, J.; Zhang, W.; Alhebshi, N. A.; Salah, N.; Alshareef, H. N. Electrochemical Zinc Ion Capacitors: Fundamentals, Materials, and Systems. *Adv. Energy Mater.* **2021**, *11*, 2100201.
10. Shang, P.; Liu, M.; Mei, Y.; Liu, Y.; Wu, L.; Dong, Y.; Zhao, Z.; Qiu, J. Urea-Mediated Monoliths Made of Nitrogen-Enriched Mesoporous Carbon Nanosheets for High-Performance Aqueous Zinc Ion Hybrid Capacitors. *Small* **2022**, *18*, 2108057.
11. Deng, X.; Li, J.; Shan, Z.; Sha, J.; Ma, L.; Zhao, N. A N, O co-doped hierarchical carbon cathode for high-performance Zn-ion hybrid supercapacitors with enhanced pseudocapacitance. *J. Mater. Chem. A* **2020**, *8*, 11617-11625.
12. Wu, S.; Chen, Y.; Jiao, T.; Zhou, J.; Cheng, J.; Liu, B.; Yang, S.; Zhang, K.; Zhang, W. An Aqueous Zn-Ion Hybrid Supercapacitor with High Energy Density and Ultrastability up to 80 000 Cycles. *Adv. Energy Mater.* **2019**, *9*, 1902915.
13. Wang, L.; Peng, M.; Chen, J.; Tang, X.; Li, L.; Hu, T.; Yuan, K.; Chen, Y. High Energy and Power Zinc Ion Capacitors: A Dual-Ion Adsorption and Reversible Chemical Adsorption Coupling Mechanism. *ACS Nano* **2022**, *16*, 2877-2888.
14. Fei, R.; Wang, H.; Wang, Q.; Qiu, R.; Tang, S.; Wang, R.; He, B.; Gong, Y.; Fan, H. J. Solid-State Electrolyte Design for Lithium Dendrite Suppression. *Adv. Energy Mater.* **2020**, *10*, 2002741.
15. Liu, Y.; Umar, A.; Wu, X. Metal-organic framework derived porous cathode materials for hybrid zinc ion capacitor. *Rare Metals* **2022**, *41*, 2985-2991.
16. Kim, M.; Xin, R.; Earnshaw, J.; Tang, J.; Hill, J. P.; Ashok, A.; Nanjundan, A. K.; Kim, J.; Young, C.; Sugahara, Y.; Na, J.; Yamauchi, Y. MOF-derived nanoporous carbons with diverse tunable nanoarchitectures. *Nat. Protoc.* **2022**, *17*, 2990-3027.
17. Kitamoto, Y.; Cao, K. L. A.; Le, P. H.; Abdillah, O. B.; Iskandar, F.; Ogi, T. A Sustainable Approach for Preparing Porous Carbon Spheres Derived from Kraft Lignin and Sodium Hydroxide as Highly Packed Thin Film Electrode Materials. *Langmuir* **2022**, *38*, 3540-3552.
18. Mao, J.; Niu, D.; Huang, G.; Jin, X.; Wei, C.; Cai, J.; Li, Y.; Shi, A Ni/Ni2P heterostructure in modified porous carbon separator for boosting polysulfide catalytic conversion. *J. Sci. China Mater.* **2022**, *65*, 2453-2462.
19. Fu, Q.; Yang, H.; Yu, J.; Li, N.; Tong, Y.; Wei, S.; Hao, Z.; Wang, J.; Ouyang, G. Porous carbon nano-sheets as excellent carbocatalysts for organic pollutant removal via persulfate activation: the role of the sp2/sp3 carbon ratio. *Environ. Sci.: Nano* **2022**, *9*, 1748-1758.

 doi:10.20944/preprints202306.1789.v1

20. Yang, B.; Chen, J.; Lei, S.; Guo, R.; Li, H.; Shi, S.; Yan, X. Spontaneous Growth of 3D Framework Carbon from Sodium Citrate for High Energy- and Power-Density and Long-Life Sodium-Ion Hybrid Capacitors. *Adv. Energy Mater.* **2018**, *8*, 1702409.
21. Yan, T.; Wang, J.; Wu, Q.; Huo, S.; Duan, H. MOF-derived graphitized porous carbon/Fe–Fe3C nanocomposites with broadband and enhanced microwave absorption performance. *J. Mater. Sci.: Mater. Electron.* **2019**, *30*, 12012-12022.
22. Wang, T.; Liu, W.; Li, M.; Hu, M.; Duan, Z.; Du, Y.; Fan, H.; Liu, S.; Jin, Y. Intercalation pseudocapacitance of hollow carbon bubbles with multilayered shells for boosting K-ion storage. *J. Mater. Chem. A* **2022**, *10*, 2075-2084.